Lawrence Berkeley National Laboratory
Recent Work

Title
Coupled THM Modeling of Hydroshearing Stimulation in Tight Fractured Volcanic Rock

Authors
Rinaldi, AP
Rutqvist, J
Sonnenthal, EL
et al.

1 COUPLED THM MODELING OF HYDROSHEARING STIMULATION IN

2 TIGHT FRACTURED VOLCANIC ROCK

3

4 A. P. Rinaldi[a], J. Rutqvist[a], E. L. Sonnenthal[a], T. T. Cladouhos[b]

5

6 (a) Lawrence Berkeley National Laboratory

7 1 Cyclotron Road

8 Berkeley, CA, 94720, USA

9 e-mail: aprinaldi@lbl.gov, jrutqvist@lbl.gov, elsonnenthal@lbl.gov

10

11 (b) AltaRock Energy

12 7900 E. Green Lake Drive N

13 Seattle, WA, 98115, USA

14 e-mail: tcladouhos@altarockenergy.com

15

16

17

18

19

20

22

23

24**ABSTRACT**

25In this study, we use the TOUGH-FLAC simulator for coupled thermo-hydro-mechanical (THM)

26modeling of well stimulation for an Enhanced Geothermal System (EGS) project. We analyze the

27potential for injection-induced fracturing and reactivation of natural fractures in a porous

28medium with associated permeability enhancement. Our analysis aims to understand how far the

29EGS reservoir may grow and how the *hydroshearing* effect depends upon system conditions. We

30analyze the enhanced reservoir, or hydrosheared zone, by studying the extent of the failure zone

31using an elasto-plastic model, and accounting for permeability changes as a function of the

32induced stresses. Results, for both fully saturated and unsaturated medium cases, demonstrate

33how the EGS reservoir growth depends on the initial fluid phase, and how the reservoir extent

34changes as a function of two critical parameters: the coefficient of friction and the permeability-

35enhancing factor. Moreover, whereas the stimulation is driven by the pressure exceeding a

36hydroshearing threshold, the modeling also demonstrates how the injection-induced cooling

37boosts the stimulation a bit farther.

38**INTRODUCTION**

39Thermo-hydro-mechanical (THM) analysis is essential when dealing with energy extraction from

40hot dry rock. The main concept of the Enhanced Geothermal System (EGS) is the exploitation of

41high thermal gradient regions through the creation (or reactivation) of a fracture network by

42increasing rock permeability, hence enhancing the circulation of water. EGS sites generally

43feature very low permeability formation (such as igneous rock in volcanic regions), where cold

44water is injected at moderate to high pressure to achieve *hydroshearing* (e.g., Cladouhos et al.,

452009). Contrary to the more common hydrofracturing (or simply *fracking*) process, during

46hydroshearing reactivation, the injection pressure is kept below the minimum principal stress

47magnitude, causing existing fractures to dilate, slip and shear. Hydroshearing can permanently

48enhance permeability of natural fractures that conceptually should remain open because of self-

49propping of fractures due to surface roughness when the stimulation period ends and fluid

50pressure is reduced. As pointed out by Riahi and Damjanac (2013), the enhancement of the

51reservoir permeability during hydroshearing will depend on many *in situ* parameters, such as

52regional stress, geological, hydromechanical, and thermal parameters (e.g., frictional coefficient,

53intact rock permeability, heat capacity), as well as chemical processes associated with the

54injection of cold water.

55

56The concept of *hydroshearing* is not new, but was first recognized and developed in the early

571980s, when Pine and Batchelor (1984) confirmed that the creation of new fractures was not the

58dominant process during the injection of water into the rock mass at great depth. Far more

59important was the shearing of natural joints and, in particular, those aligned with the principal

60stresses of the local stress field. In this concept, the joints fail in shear because the fluid injection

61reduces the normal stress across them and allows frictional slippage to occur before jacking, or

62creating of new hydraulic fractures. This was first demonstrated for the Cornwall hot dry rock

63project in the Carnmenellis granite where injection was conducted at depths greater than 2 km

64below ground level. Microseismic events detected during the high-flow rate stimulations

65indicated strike-slip shear consistent with the orientation of the natural joints and in-situ stress

66conditions. Meanwhile, in the field rock mechanics, the effects of fracture shear on permeability

67was studied through laboratory and in situ block experiments, with the first comprehensive study

68conducted at the Norwegian Getechnical Institude by Makurat et al., (1990). The concept of

69hydroshearing have since been employed at a number of EGS sites worldwide, including Hijoiro

70and Ogachi Japan as well as Soultz-sous-Forêts and Cooper Basin in Australia (Tester, 2006;

2 3

71Ziagos et al., 2013). Experience gained in the last thirty years at EGS field projects has shown

72the critical importance of understanding and mapping the natural fracture system and the in situ

73stress field (Evans et al., 1999, Tester 2006). Trans-tensional environments (e.g., grabens) may

74be more amenable to successful manipulation than compressive stress regimes in EGS reservoir

75creation (Baria et al., 1999). Moreover, in the recent few years a number of EGS demonstration

76projects have been launched in the U.S., in which different variants of hydroshearing is

77employed in stimulation and permeability enhancement of the reservoir (Ziagos et al., 2013).

78These are funded by the U.S. Department of Energy's Geothermal Technology Program and

79include EGS demonstrations at Desert Peak and Brady's Hot Springs, in Nevada, The Geysers in

80California, and finally the Newberry Volcano, Oregon (Ziagos et al. 2013). Three of these EGS

81demonstrations projects (Dessert Peak, Brady's, and The Geysers) are located within or on the

82margins of existing hydrothermal fields, whereas one (Newberry Volcano), is located at an

83unexplored and undeveloped site (Ziagos et al. 2013).

84

85In 2009, AltaRock Energy company was awarded a grant by the U.S. Geothermal Technology

86Program to plan and demonstrate an EGS at the Newberry Volcano, Oregon. During Phase I of

87the project, completed in April 2012, pre-stimulation field investigations were performed to

88understand the tectonic and volcanic setting, characterize the volume around the proposed EGS

89demonstration area, and plan the stimulation parameters. The stimulation plan was developed

90along the lines of Alta Rock Energy's approach to hydroshearing in which the rock is stimulated

91in stages by injection in multiple isolated sections of the well bore using a injection pressure that

92is slightly lower than the pressure required for hydrofracturing, i.e. slightly lower than the

93minimum principal stress (Cladouhos et al., 2009).

94

95A preliminary 3-D model of stress and fracture patterns was presented by Davatzes and Hickman

96(2011). Faulting is mainly evident along the caldera rim about 3 km from the designated

97injection well. There is no evidence of ring fractures or faults in the injection well (NWG 55-29)

98from drilling logs. Furthermore, Newberry Volcano has a very low seismicity rate (Cladouhos et

99al., 2013). An analysis of the natural fractures shows that there are two dominant sets that strike

100N-S and dip approximately 50˚ to the east and west (Davatzes and Hickman, 2011).

101The stimulation took place between October and December 2012, during which three zones were

102created by injecting thermal-degrading zonal isolation materials (chemical diverters) to isolate

103already stimulated zones (Petty et al., 2013). Over 40,000 m^3 of water were injected in about 7

104weeks of stimulation, reaching a maximum well-head pressure of about 16 MPa with over 200

105induced microseismic events registered (Petty et al., 2013; Cladouhos et al., 2013). The

106maximum magnitude event (Mw = 2.39) was recorded during the period of highest well head

107pressure (P = 16.7 MPa). However, results show a strong correlation between the cumulative

108injected volume and cumulative logarithmic seismic moment, pressure does not correlate as

109strongly. The cloud of microearthquakes extends about 500–800 m from the injection well

110(Cladouhos et al., 2013).

111A simultaneous analysis of flow rates, pressure, and seismicity that occurred at the Newberry

112EGS Demonstration site after the stimulation shows that the injectivity increased after

113reactivation, indicating an increase in permeability. The maximum well-head pressure (controlled

114at pump) resulted only after the injection of the chemical diverters, which reduced the flow rates.

115Moreover, no changes in pressure or flow rate seem to indicate the occurrence of hydrofracking

116or tensile failure, meaning that the pressure was below the minimum principal stress, but well

117within the range to achieve hydroshearing and its associated permeability enhancement.

118

119 Starting from the results obtained at Newberry Volcano, here we aim to study the hydroshearing

120 effects during stimulation at an EGS site. We use as input the same stress field and rock

121 properties (such as low permeability and porosity) measured at Newberry, and simulate the

122 stimulation using a transient well-head pressure similar to the one recorded on the field. We do

123 not aim to reproduce neither the seismicity nor the flow rate in exact detail, but aimed at a model

124 that broadly represent the conditions and injection data at the Newberry. For example, we used a

125 simplified but representative well pressure and a resulting flow rate that was similar to the

126 measured one, though not matched in great detail.

127

128 The main goal of this work is to understand how hydroshearing may occur during stimulation,

129 using the Alta Rock's hydroshearing approach (Claduohus et al., 2009). Through the use of the

130 simulator TOUGH-FLAC (Rutqvist et al., 2002), we simulate a porous medium, which deforms

131 when subjected to stress change. Fracture effect is simulated by assuming an anisotropic field of

132 permeability, with the most of the fluid flow occurring then along the assumed fracture direction.

133 Generally fracture aperture may change as subject to stress, and we simulate such a process by a

134 permeability-stress relation. Furthermore, if the stresses reach a critical value, defined by the

135 Mohr-Coulomb criterion, shear failure will occur, and the permeability of the porous medium

136 will be further enhanced by a certain factor (generally between 2 and 3 orders of magnitude –

137 Rutqvist and Stephansson, 2003). We study the extent of the EGS reservoir after the stimulation

138 (hydrosheared zone) both in a single-phase (liquid), single-component (water) system and in a

139 two-phase (gas, liquid), two-component (CO_2, water) system. Effects of some key parameters,

140 such as the frictional coefficient and a permeability-enhancing factor, are studied as well.

141**MODEL SETUP**

142The coupled THM analysis was conducted using the simulator TOUGH-FLAC (Rutqvist et al.,

1432002; Rutqvist, 2011) based on the geothermal reservoir simulator TOUGH2 (Pruess et al.,

1442011), which allows the modeling of multiphase and multicomponent fluids in a porous medium,

145and the geomechanical code FLAC3D (Itasca, 2009), for the stress changes induced by pressure

146and temperature. The TOUGH-FLAC simulator has been recently applied and tested over a wide

147range of research fields, such as carbon sequestration (e.g., Cappa and Rutqvist, 2012; Rinaldi

148and Rutqvist, 2013), nuclear waste disposal (e.g., Rutqvist and Tsang, 2012, and references

149therein), hydrothermal systems and volcanology (Todesco et al., 2004), as well as studies related

150to water injection in geothermal fields (e.g., Rutqvist et al., 2013a; Vasco et al., 2013).

151Following the approach of Rutqvist et al. (2013a) for modeling of the stimulation injection at the

152Northwest Geysers EGS Demonstration Project, we studied the stimulation at a generic EGS

153reservoir with low initial permeability, suitable for observing hydroshearing, such as at Newberry

154Volcano. Although it is beyond the aim of this paper to reproduce the data and observation

155recorded at the Newberry EGS Demonstration, we preferred to perform our simulation study of

156the hydroshearing and EGS reservoir extent starting from some reliable parameters such as those

157obtained from Newberry Volcano site, where data were collected for more than one year before

158starting the stimulation. In this study, we extended Rutqvist et al.'s (2013a) approach to calculate

159the actual permeability enhancement during the injection.

160We considered a one-quarter symmetric model, with the injection well (corresponding to the

161Newberry well NWG 55-29) located in one corner (Fig. 1). The model domain is a parallelepiped

162of dimensions 1.5 × 1.5 × 3.5 km and consists of four layers, representing the main geological

163formations of the Newberry area (Sonnenthal et al., 2012). Hydrological properties are listed in

164Table 1.

165During hydroshearing and hydrofracturing, the medium permeability changes as a result of

166injection-induced fluid pressure and effective stress changes, and is strongly dependent on *in situ*

167stress magnitude and orientation as well as fracture orientation. In this study, we consider a

168stress-dependent permeability (hence also an anisotropic initial permeability) with maximum

169permeability in the NS-direction, in order to simulate a highly fractured low permeability

170formation (such as the intruded John Day formation at the Newberry volcano).

171The injection well was simulated as a porous medium with high vertical permeability and very

172high porosity). It is divided into two sections. The first section represents a cased well (high

173vertical permeability and very low horizontal permeability), which allow heat exchange only and

174prevent fluid escaping from the well to the host rock. The second section represents an open well

175completion (very high vertical permeability and same horizontal permeability as the host rock)

176that allows the injection of cold water into the highly fractured low permeability formation

177(between 2000 m and 3000 m depth).

178Initial temperature and pressure distribution were extracted from former analyses of the pre-

179stimulation steady-state conditions at Newberry Volcano (Sonnenthal et al., 2012). The

180temperature follows a high gradient of about 100 ˚C/km, with a maximum temperature of about

181360˚C at the bottom of the domain. The pressure is slightly lower than hydrostatic, with a linear

182gradient of about 8.3 MPa/km. Constant pressure was set at the top and bottom boundaries,

183whereas side boundaries were assumed to be closed to fluid flow. No-flow side boundaries are

184needed to simulate only a quarter of a symmetric domain.

185Mechanical properties follow the results of Li et al. (2012). We chose to simulate a model with

186homogeneous mechanical properties and use a Young's modulus of $E = 15$ GPa and Poisson's

187ratio $\square = 0.3$. Homogeneous mechanical properties should be adequate in this case, since we

188simulate a short-term stimulation (slightly less than two months) that should affect only the

7   8

189injection zone (EGS reservoir). Indeed mechanical properties (such as shear and bulk modulus,

190and friction angle) may depend on medium heterogeneities, and then affect the stress and

191deformation distribution at macro scale. However, we are already accounting for an anisotropic

192permeability field, which affect the pore pressure distribution, and then the stress evolution as

193well. Random heterogeneities in mechanical properties may be present in a real field, but only at

194microscopic scale (i.e. too small to be analyzed in this study).

195Initial geomechanical conditions follow those used by Cladouhos et al. (2011) for the pre-

196stimulation analysis performed with the AltaStim simulator. We considered a vertical stress

197gradient of 24.1 MPa/km (σ_V, maximum principal stress in z-direction). The intermediate

198principal stress is oriented in the NS-direction (y-axis, σ_H) with a gradient of 23.5 MPa/km.

199Finally, the minimum principal stress is oriented in the EW-direction with a gradient of 14.9

200MPa/km (σ_h, x-axis). Thermal effects on stress were taken into account as well, choosing a

201coefficient of linear thermal expansion $\alpha_t = 10^{-5}$ °C^{-1}.

Permeability changes

203Laboratory tests have shown how the state of stress may affect the hydraulic properties in

204samples (e.g. Liu et al., 2004). Specifically, the medium permeability is related to the fracture

205mechanical aperture b and to the effective stress normal to the fracture σ_n according to the

206following exponential function (Liu et al., 2004):

207   $b = b_r + b_{max} \exp(\alpha\,\sigma_n)\quad(1)$

208where b_r is the initial mechanical aperture, b_{max} is the mechanical aperture corresponding to zero

209normal stress, α is a parameter related to the curvature of the fitting function. The mechanical

210aperture change can also be simply related to the initial state of stress (Rutqvist et al., 2008):

211   $b = b_i + b_{max}\left(\exp(\alpha\,\sigma_n) - \exp(\alpha\,\sigma_i)\right)\quad(2)$

212, and σ_{ni} is the initial stress normal to the fractures. In our formulation, compressive stresses are

213considered negative.

214

215Generally most of the EGS sites feature a fracture system striking a certain direction. The

216Newberry Volcano, for example, features a NS-striking fracture system. Such a direction would

217be the y-axis in our formulation, and by assuming an initial anisotropic permeability field in a

218porous medium (higher permeability on y-axis), we can simulate the effects of the fracture

219network. The permeability would change mostly in the fracture direction (i.e. y-axis) and

220changes will be negligible in the other directions. We can calculate the changes in permeability

221along the y-direction (κ_y) as a function of the normal stress (σ_x) using the cubic law of parallel-

222plate flow (Witherspoon at al., 1980):

223 $\quad \kappa_y = f \dfrac{b_y^3}{12} \quad (3)$

224where κ_y is the permeability in the fracture direction (y-axis in our case) and f is the fracture

225spacing. b_y is the fracture aperture from Eq. 1 or 2, and it is a function of the stress normal to the

226fracture (σ_x).

227Using the approach described by Eqs. 1-3 would require a high number of unknown parameters

228that need to be calibrated (b_r or b_i, b_{max}, f, and α). However, we can reduce the number of

229parameters by following an approach for scaling the fracture properties with the initial

230permeability (Liu et al., 2004). Following Eq. 3, we can relate the ratio between initial,

231unstressed permeability and the final permeability to the ratio between the aperture at initial state

232and aperture at final stage:

233 $\quad \dfrac{\kappa_y}{\kappa_{yi}} = \left(\dfrac{b_y}{b_{yi}}\right)^3 \quad (4)$

234then using a dimensionless parameter $R_b=b_r/b_{max}$, and combining Eq. 4 with Eq. 1, we can write

235for permeability changes (Liu et al., 2004):

$$236 \quad \frac{\kappa_y}{\kappa_{yi}}=\left[\frac{R_b+\exp\left(\alpha\sigma_x\right)}{R_b+\exp\left(\alpha\sigma_{xi}\right)}\right](5)$$

237where the stress aperture function is related to the dimensionless parameter $R_b=b_r/b_{max}$. Assuming

238the fractures to be identical, R_b will be a constant through the model domain. Using R_b, the

239permeability change factor is independent of initial permeability. We implemented Eq. 5 into

240TOUGH-FLAC and calibrate our model for two parameters only (R_b and ☐) using data recorded

241during an injection test (see following section).

242

243The variation of stress is not the only process that may affect the permeability. Most of the

244changes will occur after shear reactivation, which is the main mechanism for creating permanent

245permeability enhancement within the EGS reservoir. However, while stress-induced permeability

246changes occur everywhere in the domain along the direction of fractures subjected to aperture

247changes, the shear-induced permeability changes only occur in the portion of the domain

248subjected to shear reactivation. In this work we assumed that the permeability would change by a

249fixed factor if a gridblock were subjected to shear reactivation:

$$250 \quad \kappa_i=K_{HS}\cdot\kappa_i^{bHS}(6)$$

251for the i-direction. K_{HS} is a constant value (set to 500 for the base case analyses, i.e., between 2

252and 3 orders of magnitude), and the index bHS refers to the permeability before the

253hydroshearing. Reactivation may occur with random orientation if a threshold pressure is

254reached, then we cannot attribute the changes in a single direction, but we assume the

255permeability changes isotropically if shear reactivation occur.

256 In case of multi-stage shearing, the permeability changes accordingly, i.e. the permeability κ^{bHS}

257 represents the one before the actual shear stage.

258 A similar approach was also recently used by Kelkar et al. (2012) during the study of shear

259 stimulation at Desert Peak Geothermal Field (Nevada), though limiting the permeability change

260 to a factor of 15 upon shear failure.

261

262 Alternative approaches for modeling hydroshear may involve discrete fracture network models

263 or combinations of fracture network and continuum models. For example when using the distinct

264 element codes 3DEC or UDEC in which each fracture is explicitly represented, the permeability

265 changes in individual rock fractures may be calculated as a result of aperture changes due to

266 shear induced dilation based on some constitutive law for single fractures (e.g Min et al. 2004).

267 Other examples involve discrete fracture network models originally developed for groundwater

268 flow and transport extended through a simplified geomechanics approach in which shear failure

269 on each fracture is evaluated in an assumed and constant and homogenous external stress field

270 (e.g. Willis-Richards 1996; Bruel, 2007). In such an approach, the fracture responses upon shear

271 failure may be calculated based on a local elastic solution for an assumed circular shaped

272 fracture of certain radius. For example, based on the radius of the fracture and shear modulus of

273 the surrounding rocks, the shear stress drop and maximum shear displacement and associated

274 fracture dilation and permeability change can be calculated. Such an approach has the potential

275 of handling a large number of fractures explicitly, but the mechanics is simplified as described

276 and does not consider shear induced stress changes or relaxation of the stress field in stimulated

277 areas. A combination approach may involve considering a back-ground fracture network used for

278 calculating equivalent continuum properties that for a very fine continuum mesh can be used to

279 represent fractures explicitly by changing properties of elements that are intersected by

280 individual fractures surfaces (Tezuka et al., 2005; Rutqvist et al., 2013b). The approach for

281 permeability change adopted in this study can be considered a rational approach applied to a

282 continuum model. However, regardless of the model adopted it usually involves some level of

283 calibration against field data as will be discussed in the next section.

284

285 **Model calibration**

286 Model calibration is necessary for understanding whether the system is correctly responding to

287 the injection of fluids and whether boundary and initial conditions are properly set.

288 Pore compressibility (c_p) and thermal conductivity ($\square$) within the injection well were calibrated

289 to match field data. Moreover, a calibration is needed to assign appropriate values to the

290 parameters $\square$ and R_b for the stress-dependent permeability function (Eq. 5).

291 The calibration was made simulating a low-pressure injection test, and comparing the resulting

292 pressure and temperature profiles along the well with data collected at the NWG 55-29 well

293 during a field injection test (September-October 2010).

294 According to Davatzes and Hickman (2011) the injection test was performed in two steps.

295 During the first period, lasting three days, the injection rate was 0.6 L/s (10 gpm) with an

296 injection temperature of 10°C and a well-head pressure of about 5 MPa (750 psi). This period

297 was then followed by two weeks of shut-in, before restarting the injection for nine days at a rate

298 of 1.4 L/s (22 gpm), with an injection temperature of 10°C and a wellhead pressure of about 8

299 MPa (1153 psi).

300 Here we performed a simulation with the same, transient injection and we reproduced the same

301 observed profiles along the well for pressure and temperature after 3 days at 10 gpm (Fig. 2a and

302 b for pressure and temperature, respectively) and after 9 days at 22 gpm (Fig. 2c and d, for

303 pressure and temperature, respectively), considering the permeability changes that may arise

12   13

304with the evolving effective stresses. Parameters for permeability changes were set constant

305during the two stages as $R_b = 0.2$ and $\square = 0.13$ MPa^{-1} after calibration (see Eq. 5). The calibration

306for R_b and $\square$ is not unique, but the used of the two parameters only reduce the degree of freedom

307of the system.

308The pore compressibility and thermal conductivity were calibrated as well, and the values

309allowing a good match between simulated and measured profiles are listed in Table 1. As stated

310by Davatzes and Hickman (2011), after nine days of 22 gpm injection the well-head pressure was

311lowered to allow the well to be logged; hence, the pressure field data in Figure 2d needs to be

312recalibrated to match a wellhead pressure of 8 MPa (1153 psi) during the majority of the inject-

313to-cool operation.

314**STIMULATION AND HYDROSHEARING MODELING**

315The stimulation of an EGS reservoir requires that an elevated amount of water be injected into

316the system. For example, at the Basel geothermal system (Switzerland) more than 11500 m^3 of

317water were injected in about 5 days (about 30 L/s average flow rate) before peaking at a well-

318head pressure of almost 30 MPa and inducing a $M_L = 3.4$ event (Bachmann et al., 2011). In

319contrast, at the Northwest Geysers EGS Demonstration at The Geysers Geothermal Field

320(California), flow rates reached more than 50 L/s, but bottom-hole pressures were relatively low

321(typically less than 8 MPa), resulting in a large number of small-magnitude seismic events and a

322maximum magnitude event of 2.87 (Garcia et al., 2012; Vasco et al., 2013; Rutqvist et al. 2013a).

323Flow rates during the stimulation at the Newberry EGS Demonstration ranged from about 5 L/s

324up to 20 L/s, with a well-head pressure that peaked at about 16 MPa (Fig. 3, Petty et al., 2013).

325The stimulation was conducted in three different stages, and thermally degradable zonal isolation

326materials (TZIM) were injected between each stage to partially seal stimulated permeable

327fractures and activate stimulation in a new zone. The use of chemical diverters (TZIM) helped to

328stimulate multiple zones in the well bore, resulting then in a more injection or flow capacity (last

329ten days in Fig. 3). Detailed description of the three stages performed during the stimulation can

330be found in Petty et al. (2013).

331Here we are interested in the effects of the stimulation on hydroshearing and how far EGS

332reservoirs can extend under different system conditions. In most of the EGS applications,

333operators try to maintain a fixed injection rate, monitoring the injection pressure as outcome.

334However, we preferred to keep the pressure constant rather the injection rate, since the pressure

335is the main variable for reactivation. There was no fundamental reason, and it was done for better

336understanding of the process of hydroshearing, which is mainly based on pressure rather than on

337the flow rate. The stimulation injection is simulated by fixing the pressure at the top of the well,

338following the average values recorded at the Newberry Volcano EGS Demonstration. Again, it is

339not our goal to reproduce the observed injectivity and flow rates in detail, but it is essential to

340keep our model as close as possible to a real case, in order to achieve reasonable simulation

341results (Fig. 3).

342We simulated the injection in two stages. The first stage lasted for about 28 days with a fixed

343well-head pressure of 7.8 MPa. This is followed by a 10 day shut-in period, before the injection

344restarts for the second stage with 3 days at 7 MPa and 10 days at 14 MPa (Fig. 3, green line).

345Note that we did not consider the effect of diverters (TZIM), which means that an increase in

346pressure results in an increase in flow rate, whereas, as observed at Newberry, the diverters

347sealed the permeable zones, permitting an higher well-head pressure without a substantial

348increase in flow rate prior to the start of subsequent stimulation steps.

349The increase in pressure is necessary to allow the system to reduce the shear strength of fractures

350to less than the shear stress across the fracture, and enable the hydroshearing of fractures with a

14   15

351wider variety of fracture orientations to occur (Cladouhos et al, 2011). Rather than keeping a

352fixed, high value for the well-head pressure, we preferred to study a case of transient evolution,

353in which the injection starts at a relatively low pressure (7 MPa, first stage) and then is doubled

354after a shut-in (no-injection) period (14 MPa, second stage). The values we chose are within the

355range needed for hydroshearing, but never exceeded the minimum principal stress, so that only

356shear failure can occur, rather than tensile failure or fracturing.

357To estimate the extent of the EGS reservoir, we looked at the zone where the system is subjected

358to hydroshearing. This can be done with a Mohr-Coulomb model: considering a cohesionless

359solid, shear reactivation will occur when the following criterion is satisfied:

360 $\quad \sigma_{1c}' = N_\phi \sigma_3', N_\phi = \dfrac{1+\sin\phi}{1-\sin\phi}\,(7)$

361where σ'_{1c} is the critical maximum principal effective stress (σ'_V or σ'_{zz} in our case), and σ'_3 is the

362minimum principal effective stress (σ'_h or σ'_{xx}). ϕ is the frictional angle (frictional coefficient

363$\mu=\tan\phi$), which is set to 30° for the base-case simulation. In our model we considered as Mohr-

364Coulomb solid the Intruded John Day formation only, and the upper John Day formation, which

365is not a highly fractured formation, acts as a barrier for fracture propagation (Fig. 1). This may

366not be true in the field, and the fractures may propagate to shallow depth.

367Equation 7 corresponds to the case in which the media contains fractures with a uniform

368distribution of orientations and equally spaced throughout the reservoir. Using this approach,

369shear reactivation would be induced whenever the maximum principal stress is N_ϕ times higher

370than the minimum principal stress.

371**Stimulation of a single phase, single component system**

372The first model we analyze does not take into account the presence of gas within the system.

373Basically, we simulated the stimulation of a geothermal system injecting water into a fully water-

374saturated system. We are fully aware that this is a limiting case in this high temperature

375environment, but would certainly be applicable in lower temperature systems. For this base case

376the friction angle ⬜ was set to 30˚, i.e., a standard value corresponding to a frictional coefficient

377of about 0.6. The constant K_{HS} for shear-enhanced permeability changes was set to 500, i.e.

378corresponding to a 2.7-order magnitude change in permeability to all directions when a shear

379reactivation occurs. This constant was set to a sensible value (Rutqvist and Stephansson, 2003).

380For example, Lee and Cho (2002) have shown after laboratory tests that two orders magnitude

381increase in fracture permeability may arise upon shear displacement.

382Figure 4a shows the pressure transient evolution applied at the top of the injection well (red line)

383and the resulting flow rate associated with the water-saturated system (blue line). Results show a

384first period during which the flow rate increases up to about 30 kg/s, then hydroshearing begins

385occurring and the flow rate stabilizes to a constant value of about 20 kg/s (or L/s) for the rest of

386the first stage (0 – 28 days with well-head pressure at 7.8 MPa). During the 10 day shut-in

387period, the flow rate is almost nil. Then, during the second stage of stimulation, the well-head

388pressure reaches 14 MPa, and the flow rate peaks at more than 60 kg/s, only to decrease to 40

389kg/s at the end of the stimulation. The simulated flow rates are similar to values observed at EGS

390demonstration sites such as The Geysers (Rutqvist et al., 2013a; Vasco et al., 2013) and

391Newberry Volcano (Petty et al., 2013). Again, note that we are not simulating any injection of

392diverters, and then, during our second stage of the stimulation for a higher well-head pressure,

393we achieve a higher flow rate. The use of diverters proved to be effective at Newberry, where the

394sealing properties of the injected isolating materials sealed the existing permeable fracture

395network, thus resulting in higher pressures but with the same flow rate (Petty et al., 2013).

396Results for pressure changes within the system, and the resulting zone affected by shear

397reactivation after 28 days of stimulation, are shown in Figure 4b and c, respectively. Pressure

16   17

398changes and the hydrosheared zone both extend up to about 400 m from the injection well in the

399NS direction (*y*-axis), i.e., along the direction we set as the primary fracture strike, which has

400higher permeability (Table 1). Growth of the hydrosheared zone is much smaller in the EW

401direction (*x*-axis), since both the initial permeability and the stress-induced permeability changes

402are smaller in the EW direction, which means that pressure changes do not propagate much in

403that direction. Although the pressurization within the well reaches about 8 MPa (same as the

404wellhead pressure during this first stage), within the system the pressure changes are a few MPa

405smaller, reaching a maximum of 6 MPa at the bottom of the well (Fig. 4b). However, these few

406MPa changes are enough to satisfy the failure criterion and activate the shearing process (Fig.

4074c).

408After the second stage, the increased well-head pressure results in higher-pressure changes

409within the system. In fact, Figure 4d shows the changes to be around 6 MPa, with maximum

410value of 8 MPa in the region close to the bottom of the well, although these values are still a little

411smaller than the pressure change within the well (about 12 MPa). The resulting hydrosheared

412region expands somewhat during the second stage, reaching a maximum value of about 500 m

413along the NS-direction (Fig. 4e). We can estimate the extent of the EGS reservoir and calculate

414the volume of the region affected by pressure change and where reactivation occurred: such a

415stimulated volume corresponds to about $9 \cdot 10^7$ m^3, i.e., about 0.1 km^3.

416**Stimulation of a two phase, two component system**

417In this section, we consider a system that before the stimulation is completely dry, saturated with

418gaseous CO_2, subjected to cold-water injection. Hydrological and mechanical properties were

419kept the same as the fully water-saturated case. We used an equation of state for a two-

420components system (CO_2 and water – EOS2). Carbon dioxide can dissolve in water according to

421the Henry's law and the equation of state is applicable up to the water critical temperature (350

17   18

422°C), although it does not account for chemical reaction. More details can be found elsewhere

423(Pruess et al., 2011).

424This conceptual model may be somewhat unrealistic, but it represents a good case study as

425compared to the previous water-saturated system. Moreover, CO_2 is a good approximation for a

426volcanic gas: there are a few examples in literature of CO_2 degassing in volcanic regions, such as

427Campi Flegrei caldera (Italy) (e.g. Todesco et al., 2004) or Furnas (Azores) (e.g. Rinaldi et al.,

4282012). As previously implemented, we set the friction angle to 30° and the shear-enhanced

429permeability-changes factor to 500.

430Results of the stimulation for this system involving two fluid phases and two fluid components

431are shown in Figure 5. The pressure transient evolution imposed at the well is the same as

432previously (red line, Fig. 5a), and only a few changes are evident in the resulting flow rate

433compared to the case of a water-saturated system (blue line, Fig. 4a and 5a). The small variations

434are at the beginning of the simulation, during which a system with gas requires a higher flow rate

435to displace the gas from the region close to the injection well.

436The resulting pressure increase after the first stage (28 days) is still close to the injection well,

437with an average value of about 5 MPa (Fig. 5c). Although the pressure changes do not propagate

438far from the injection well, the average variation is still similar to the previous water-saturated

439case (Fig. 4b). As a consequence of the poorly distributed pressure changes, at this stage the

440region affected by hydroshearing is limited to a small region around the injection well and

441extends only for about 60 m along NS direction and 13 m along EW direction (Fig. 5d).

442After the second stage (51 days), the pressure changes are still averaging around 5 MPa,

443although within the well the pressure is 14 MPa (Fig. 5d). In any case, at this stage the pressure

444perturbation propagated more, resulting in a larger region where the shear reactivation occurred.

18   19

445The hydrosheared region extends about 100 m along the NS direction and about 25.5 m along the

446EW direction (i.e., almost twice that after the first stage, Fig. 5e).

447The results suggest that fractures will propagate much less in a medium initially saturated with a

448compressible gas. In fact, the stimulated volume resulting for an unsaturated medium is about

449$10^7$ m^3, i.e., about 1 order magnitude smaller than the volume that can be stimulated in a medium

450fully saturated with water. This effect can be explained because of the compressibility of the gas

451phase. In a saturated medium, the water within the system is pushed away from the volume that

452is injected, allowing for the pressure perturbation to move faster, thus reactivating a larger

453region. In an unsaturated medium, the gas phase will be compressed by the injected water. The

454injected water will propagate only to a region close to the injection well, with the pressure

455perturbation following the water front, resulting in the stimulation of a much smaller region.

456**Thermal effects on hydroshearing**

457The injection of cold water produces changes in temperature distribution. The changes are

458mostly confined around the injection well, and extend only a few tens of meters, with changes up

459to more than 30 ˚C. Resulting temperature distribution for both the water-saturated and

460unsaturated cases are shown in Figure 6a and c, respectively. Although we have seen how the

461hydrosheared zone can differ between a water-saturated and an unsaturated system, changes in

462temperature are very similar, as already showed for the resulting flow rates (Fig. 4a and Fig. 5a).

463However, these small and confined changes in temperature may have an effect on the resulting

464stress. In essence, the cooling caused by the injection along the permeable (stimulated) zone

465causes cooling shrinkage that in turn tends to cause an additional reduction in effective stress and

466shear strength. Such shear strength reduction will tend to promote shear failure and propagation

467of the stimulation zone. In fact, if we compared a case that considered a hydro-mechanical (HM,

468i.e. considering $\square_t = 0$) coupling only with a full THM modeling, we found that the temperature

469changes may help the EGS reservoir growth. In fact, the when conspiring thermal effects, EGS

470reservoir grow about 100 m farther along the NS direction for the case of water-saturated system

471(Fig6b, THM brown, HM yellow). Some small differences are observed for the case of gas-

472saturated system, with about 20 m difference between THM and HM modeling, with a slightly

473larger reservoir when thermal effects are taken into account (Fig6d).

474**Sensitivity analysis**

475We have seen how two systems can respond differently to stimulation if we account for the

476presence of gas. However, the presence of gas within a system is only one of the parameters that

477should be taken into account when simulating a complex system such as a geothermal reservoir.

478Some of the parameters can be taken from field studies: for example, the stress field, which plays

479a huge role in shear reactivation, can be evaluated by *in situ* tests, and by looking at local

480seismicity. The same can be done for the permeability, although most of the parameters studied

481in the laboratory analysis can produce results quite different from those observed in the field.

482Here, we aim to focus only on two main parameters that affect the resulting stimulated volume:

483(1) the constant K_{HS} for the shear-enhanced permeability (Eq. 6) and (2) the frictional angle ⬜ for

484the Mohr-Coulomb criterion (Eq. 7). All the analyses presented in this section were done at the

485end of the second stage, i.e., after 51 days of simulation.

486In the base-case simulations we set a shear-enhanced permeability change factor to achieve

487between a 2 and 3 orders magnitude change (K_{HS} = 500). However, in the field this factor may be

488greater (or smaller), leading to a different system response. Figure 7a shows how the EGS

489reservoir extent varies along the NS direction as a function of this constant for both an

490unsaturated (red line) and saturated system (blue line). Figure 7b shows the stimulated volume as

491a function of the shear-enhanced permeability factor. The extent of the region subject to

492hydroshearing may reach up to 800 m in a water-saturated system, when we consider a factor 10^4

493 of permeability changes, or may extend for few tens of meters when we do not consider changes

494 in permeability due to hydroshearing ($K_{HS} = 0$). These variations are much smaller for an

495 unsaturated system. Even if we use a factor 10^4, in a system that is initially gas-dominated, the

496 reservoir may extend up to about 200 m only. From both Figures 7a and b, we found that the

497 hydrosheared region (extent or volume) varies as a logarithmic function of the shear-enhanced

498 permeability factor greater than 10 (i.e. $\log_{10}(K_{HS})$ greater than one):

499 $\quad V_{HS}(L_{EGS}) \ \log_{10}(K_{HS})(K_{HS})(5)$

500 where V_{HS} represents the volume subjected to hydroshearing, which is proportional to the EGS

501 reservoir length (L_{EGS}). Note the logarithmic scale that Figure 7b.

502 The second parameter for which we perform a sensitivity analysis is the friction angle. For the

503 base-case simulations, we used an angle of 30˚, which means a friction coefficient of about 0.6.

504 This factor can play a big role, depending upon the initial stress condition. Considering a fixed,

505 linear stress distribution, with no heterogeneities and variation in depth, the friction angle simply

506 regulates how much overpressure is needed to satisfy the failure criterion (Eq. 7). Results of the

507 sensitivity analysis for this parameter are shown in Figures 6c and d, for the EGS extent along

508 the NS direction and for the stimulated volume, respectively. Both these variables seem to

509 change linearly with the friction angle, with values ranging between 600 m (volume $2 \cdot 10^8 \ m^3$)

510 and 250 m (volume $5 \cdot 10^7 \ m^3$) for a water-saturated medium with an increase in the friction angle

511 resulting in a smaller stimulated volume and linear extent, and hydrosheared region is almost

512costant for an unsaturated medium: only a 40 m variation in EGS extent over the considered

513range of values.

CONCLUSIONS

515During stimulation of an Enhanced Geothermal System (EGS) it is always difficult to predict

516how far the reservoir and fracture network can grow. Moreover, creating a new fracture network

517requires elevated pumping pressure and flow rates in order to fracture the rock. One mechanism

518that has been proposed to reduce the cost is so-called *hydroshearing*, which involves reactivating

519an existing fracture network by a shear process, taking advantage of the fracture surface

520roughness, which should naturally maintain the enhanced permeability. The pressure needed for

521hydroshearing has to be below the minimum principal stress, but without exceeding it, thus

522avoiding then the creation of new tensile fractures. Once the fractures are reactivated, some

523isolating, thermally degrading material may be injected to plug the fracture network, and this will

524permit stimulating multiple fracture zone without drill rig or setting multiple packers. Moreover,

525the injection of chemical diverters will permit injecting at a higher pressure (hence reactivating

526some other, deeper zones) without changing the flow rate.

527However, some questions need to be answered: will the presence of gas within the system help or

528reduce the hydroshearing reactivation? How much can the permeability change after reactivation,

529and how is that change related to the extent of the EGS reservoir and to the stimulated volume?

530The aim of this paper was to answer to these questions. Through the use of the TOUGH-FLAC

531simulator, we carried out a coupled thermo-hydro-mechanical modeling of EGS stimulations. We

532accounted for a Mohr-Coulomb solid that can fail when a criterion is satisfied. Upon fracture

533reactivation, we assumed a change in medium permeability, which allows for a better

534propagation of the pressure perturbation. Taking into account previous simulations performed for

535The Geysers Geothermal Field and starting with data collected at the Newberry Volcano EGS

536Demonstration site, we simulated the stimulation by fixing the overpressure at the top of an

537injection well. Pressure transient evolution was taken as the average of field values measured at

538Newberry Volcano during stimulation. Although our aim was not to reproduce any observed

539variations, we used field data to keep our model as realistic as possible.

540We first presented the results for two limiting cases: (1) a water-saturated medium and (2) a

541medium initially saturated with CO_2 in the gas phase. Results suggest that an EGS reservoir will

542extend much further in a medium initially fully saturated with water than in a gas-phase

543dominated system. We explained this effect as owing to the compressibility of the gas phase. In a

544water-saturated medium, the native water within the system is pressurized by the water injected

545into the well, allowing the pressure perturbation to propagate faster and reactivating fractures

546over a larger region. In an unsaturated medium, the much more compressible gas phase will be

547compressed by the injected water, which will propagate only to a region close to the injection

548well, following the water front, finally stimulating a much smaller region. Thermal effects on

549stress may help to reach shear failure. Although temperature changes are small and confined

550within tens of meter from the injection well, thermal effects on stress are evident at earlier time

551and helped the EGS reservoir to grow. A hydro-mechanical modeling resulted in smaller

552hydrosheared region after the stimulation.

553The presence of gas is not the only parameter affecting the growth of an EGS reservoir. Many

554parameters are involved that may play a significant role, such as the medium initial permeability,

555the natural fracture-network orientation, and the stress distribution. We performed a sensitivity

556analysis on two key parameters that are generally hard to measure in the field: (1) the factor for

557the shear-enhanced permeability changes and (2) the friction angle for the failure criterion.

558Results showed that the extent of the EGS reservoir and the volume subjected to shear

559reactivation strongly depend upon these two parameters. We found that in our system, the EGS

560extent (or reactivated region volume) will depend logarithmically upon the constant used to

561relate permeability change associated with hydroshearing, and linearly upon the frictional angle.

562These variations are more accentuated in a water-saturated system.

563The volume subjected to hydroshearing (stimulated volume) ideally should also represent the

564region where the microseismicity cloud should be. However, natural-system heterogeneities in

565the stress field and permeability may play a significant role, and the seismicity cloud may not

566exclusively represent only the region that has been stimulated. For example, a brittle material at

567shallow depth may be affected by deformation and stress transfer coming from a deeper

568overpressure, and seismicity may then be induced at a shallower depth than we would expect.

569Technical issues may be involved as well: for example, a leakage from the cased well may allow

570the water to move at shallow depths, where it is much easier to cause hydroshearing, or

571hydrofracturing, since the *in situ* would be stress smaller, generally depending on the depth.

580**REFERENCES**

581

24   25

582Bachmann, C. E., S. Wiemer, J. Woessner, S. Hainzl, Statistical analysis of the induced Basel

5832006 earthquake sequence: Introducing a probability-based monitoring approach for Enhanced

584Geothermal System, *Geophys. J. Int.,* 186(2) (2011). doi:10.1111/j.1365-246X.2011.05068.x.

585

586Baria R, Baumgärtner J, Rummel F, Pine RJ, Sato Y (1999a) HDR/HWR reservoirs: concepts,

587understanding and creation. Geothermics 28:533–552.

588

589Bruel, D., 2007, Using the migration of the induced seismicity as a constraint for fractured hot

590dry rock reservoir modeling: International Journal of Rock Mechanics and Mining Sciences &

591Geomechanics Abstracts, 44, 1106–1117.

592

593Cappa, F., J. Rutqvist, Seismic rupture and ground accelerations induced by CO_2 injection in the

594shallow crust, *Geophys. J. Int.,* 190, 1784-1789 (2012).

595

596Cladouhos, T. T., M. Clyne, M. Nichols, S. Petty, W. L. Osborn, L. Nofziger, Newberry Volcano

597EGS Demonstration Stimulation Modeling, *GRC Transactions*, 35 (2011).

598

599Cladouhos, T. T., W. L. Osborn, S. Petty, D. Bour, J. Iovenitti, O. Callahan, Y. Nordin, D. Perry,

600P. L. Stern, Newberry Volcano EGS Demonstration – Phase I results, *Proceedings of 37th*

601*Workshop on Geothermal Reservoir Engineering,* Stanford, California, January 30 – February 1,

6022012.

603

604Cladouhos, T. T., S. Petty, B. Larson, J. Iovenitti, B. Livesay, R. Baria, Toward More Efficient

605Heat Mining: A Planned Enhanced Geothermal System Demonstration Project, *GRC*

606*Transactions*, 33, 165-170 (2009).

607

608Cladouhos, T. T., S., Petty, Y. Nordin, M. Moore, K. Grasso, M. Uddenberg, M. Swyer, B. Julian,

609G. Foulger, Microseismic Monitoring of Newberry Volcano EGS Demonstration, *Proceedings of*

610*the 38th Workshop on Geothermal Reservoir Engineering*, Stanford, California, February 11 - 13,

6112013.

612

613Davatzes N. C. and S. H. Hickman, Preliminary Analysis of Stress in the Newberry EGS Well

614NWG 55-29, *GRG Transactions*, 35, 323-332 (2011).

615

616Evans KF, Cornet FH, Hashida T, Hayashi K, Ito T, Matsuki K, Wallroth T (1999) Stress and

617rock mechanics issues of relevance to HDR/WDR engineered geothermal systems: review of

618developments during the past 15 years. Geothermics 28:455–474

619

620Garcia, J., Walters, M., Beall, J., Hartline, C., Pingol, A., Pistone, S., and Wright, M., Overview

621of the Northwest Geysers EGS demonstration project, *Proceedings of the 37th Workshop on*

622*Geothermal Reservoir Engineering*, Stanford, California, January 30 – February 1, 2012

623

624Kelkar, S., K. Lewis, S. Hickman, N. C. Davatzes, D. Moos, G. Zyvoloski, Modeling coupled

625thermal-hydrological-mechanical processes druing shear stimulation of an EGS well,

626*Proceedings of the 37th Workshop on Geothermal Reservoir Engineering*, Stanford, California,

627January 30 - February 1, 2012.

628

629Lee, H. S., and T. F. Cho, Hydraulic Characteristic of Rough Fractures in Linear Flow under

630Nomrla and Shear Load, *Rock Mech. Rock Eng.*, 35 (4), 299-318, 2002.

631

632Li, Y., J. Wang, W. Jung, A. Ghassemi, Mechanical Properties of Intact Rock and Fractures in

633Welded Tuff from Newberry Volcano, *Proceedings of 37th Workshop on Geothermal Reservoir*

634*Engineering*, Stanford, California, January 30 – February 1, 2012.

635

636Liu, H. H., J. Rutqvist, G. Zhou, G. S. Bodvarsson, Upscaling of normal stress-permeability

637relationship for fracture network obeying the fractional levy motion. In: Stephansson O., Hudson

638J. A., Jing L., editors. *Coupled THMC processes in geo-system: fundamentals, modelling,*

639*experiments and applications*. Oxford: Elsevier; p.263-268 (2004).

640

641Itasca, *FLAC3D, Fast Lagrangian Analysis of Continua in 3 Dimensions, Version 4.0,*

642Minneapolis, Minnesota, Itasca Consulting Group (2009).

643

644Makurat A, Barton N, Rad NS (1990) Joint conductivity variation due to normal and shear

645deformation. In: Barton N, Stephansson O (eds) Rock joints. Balkema, Rotterdam, pp 535–540

646

647Min KB, Rutqvist J., Tsang C.-F., and Jing L. Stress-dependent permeability of fracture rock

648masses: a numerical study. *Int. J. Rock Mech. & Min. Sci*, 41, 1191-1210 (2004).

649

650Petty, S., Y. Nordin, W. Glassley, T. T. Cladouhos, M. Swyer, Improving Geothermal Project

651Economics with Multi-Zone Stimulation: Results from the Newberry Volcano EGS

652Demonstration, *Proceedings of the 38th Workshop on Geothermal Reservoir Engineering,*

653Stanford, California, February 11 - 13, 2013.

654

655Pine RJ, Batchelor AS (1984) Downward migration of shearing in jointed rock during hydraulic

656injections. Int J Rock Mech Mining Sci 21:249–263

657

658Pruess, K., C. M. Oldenburg, and G. Moridis, *TOUGH2 User's Guide, Version 2.1*, Report

659LBNL-43134 (revised), Lawrence Berkeley National Laboratory, Berkeley, Calif. (2011).

660

661Riahi, A., B. Damjanac, Numerical Study of Hydro-Shearing in Geothermal Reservoirs with a

662Pre-Existing Discrete Fracture Network, *Proceedings of the 38th Workshop on Geothermal*

663*Reservoir Engineering,* Stanford, California, February 11 - 13, 2013.

664

665Rinaldi, A. P., J. Rutqvist, Modeling of deep fracture zone opening and transient ground surface

666uplift at KB-502 CO_2 injection well, In Salah, Algeria, *Int. J. Greenh. Gas Contr.*, 12, 155-167

667(2013). doi:10.1016/j.ijggc.2012.10.017.

668

669Rinaldi, A. P., J. Vandemeulebrouck, M. Todesco, F. Viveiros, Effects of atmospheric conditions

670on surface diffuse degassing, *J. Geophys. Res. - Solid Earth*, 117, B11201 (2012).

671doi:10.1029/2012JB009490.

672

673 Rutqvist, J., Status of TOUGH-FLAC simulator and recent applications related to coupled fluid

674flow and crustal deformations. *Comput. Geosci.*, 37, 739-750 (2011).

675

676Rutqvist J., Dobson P.F., Garcia J., Hartline C., Jeanne P., Oldenburg C.M., Vasco D.W., Walters

677M. The Northwest Geysers EGS Demonstration Project, California: Pre-stimulation Modeling

678and Interpretation of the Stimulation. Mathematical Geosciences, In press, (2013a)

679

680Rutqvist J., Leung C., Hoch A., Wang Y., and Wang Z. Linked multicontinuum and crack tensor

681approach for modeling of coupled geomechanics, fluid flow and transport in fractured rock.

682International Journal of Rock Mechanics and Geotechnical Engineering, 5, 18–31 (2013b)..

683

684Rutqvist, J., B. Freifeld, K.-B. Min, D. Elsworth, Y. Tsang, Analysis of thermally induced

685changes in fractured rock permeability during 8 years of heating and cooling at the Yucca

686Mountain Drift Scale Test, *Int. J. Rock Mech. Min. Sc.*, 45, 1373-1389 (2008).

687

688Rutqvist, J., O. Stephansson, The role of hydromechanical coupling in fractured rock

689engineering, *Hydrogeology Journal*, 11 (1), 7-40 (2003).

690

691Rutqvist, J., C. F. Tsang, Multiphysics processes in partially saturated fractured rock:

692Experiments and models from Yucca mountain, *Rev. Geophys.*, 50(3) (2012).

693doi:10.1029/2012RG000391.

694

695Rutqvist, J., Y.-S. Wu, C.-F. Tsang, G. Bodvarsson, A modeling approach for analysis of coupled

696multiphase fluid flow, heat transfer, and deformation in fractured porous rock, *Int. J. Rock Mech.*

697*Min. Sc.*, 39, 429-442 (2002).

698

699Sonnenthal, E. L., N. Spycher, O. Callahan, T. Cladouhos, and S. Petty, A thermal-hydrological-

700chemical model for the Enhanced Geothermal System Demonstration Project at Newberry

701Volcano, Oregon, *Proceedings of the 37th Workshop on Geothermal Reservoir Engineering*,

702Stanford, California, January 30 - February 1, 2012.

703

704Tester, J.W. et al., 2006 The future of geothermal energy. Part 1—Summary and part 2—Full

705report. Massachusetts Institute of Technology, Cambridge, MA.

706

707Tezuka K., Tamagawa T., and Watanabe K. 2005. Numerical Simulation of Hydraulic Shearing in

708Fractured Reservoir. Proceedings World Geothermal Congress 2005. Antalya, Turkey, 24-29

709April 2005

710

711Todesco, M., J. Rutqvist, G. Chiodini, K. Pruess, C. M. Oldenburg, Modeling of recent volcanic

712episodes at Phlegrean Fields (Italy): geochemical variations and ground deformation,

713*Geothermics*, 33, 531-547 (2004).

714

715Vasco, D. W., J. Rutqvist, A. Ferretti, A. Rucci, F. Bellotti, P. Dobson, C. M. Oldenburg, J.

716Garcia, M. Walters, C. Hartline, Monitoring deformation at The Geysers geothermal field,

717California using C-band and X-band Interferometric Synthetic Aperture Radar, *Geophys. Res.*

718*Lett.*, accepted for publication (2013). doi:10.1002/grl.50314.

719

720Willis-Richards, J., K.Watanabe, and H. Takahashi, 1996, Progress toward a stochastic rock

721mechanics model of engineered geothermal systems: Journal of Geophysical Research, 101, 17,

722481–17, 496.

723

724Witherspoon, P. A., J. S. Y. Wang, K. Iwai, J. E. Gale, Validity of cubic law for fluid flow in a

725deformable rock fracture, *Water Resour. Res.*, 16, 1016-1024 (1980).

726

727Ziagos J., Phillips B.R., Boyd L., Jelacic A., Stillman G. and Eric Hass E. A technology roadmap

728for strategic development of enhanced geothermal systems. Proceedings of the 38th Workshop on

729Geothermal Reservoir Engineering , Stanford, California, February 11 - 13, 2013.

730

731**Tables**

732*Table 1*. Hydrological properties. κ_i initial (stress-free) permeability along *i*-direction. ϕ porosity.

733ρ_{rock} rock density. *D* rock grain specific heat. λ thermal conductivity. c_p pore compressibility

|	Newberry-Deschutes	John Day	Intruded John Day	Cased well	Open well
κ_x (m^2)	10^{-17}	$2.6 \cdot 10^{-16}$	$5 \cdot 10^{-18}$	10^{-20}	10^{-16}
κ_y (m^2)	10^{-17}	$2.6 \cdot 10^{-16}$	10^{-17}	10^{-20}	10^{-16}
κ_z (m^2)	10^{-17}	$2.6 \cdot 10^{-16}$	$5 \cdot 10^{-18}$	10^{-8}	10^{-8}
ϕ (%)	10	5	3	95	100
ρ_{rock} (kg/m^3)	2400	2400	2400	-	-
D (J/kg ˚C)	1000	1000	1000	800	800
λ (W/m ˚C)	1.80	2.15	2.20	2.20	1.80
c_p (Pa^{-1})	$3.2 \cdot 10^{-9}$	$3.2 \cdot 10^{-9}$	$3.2 \cdot 10^{-9}$	-	-

Figure captions
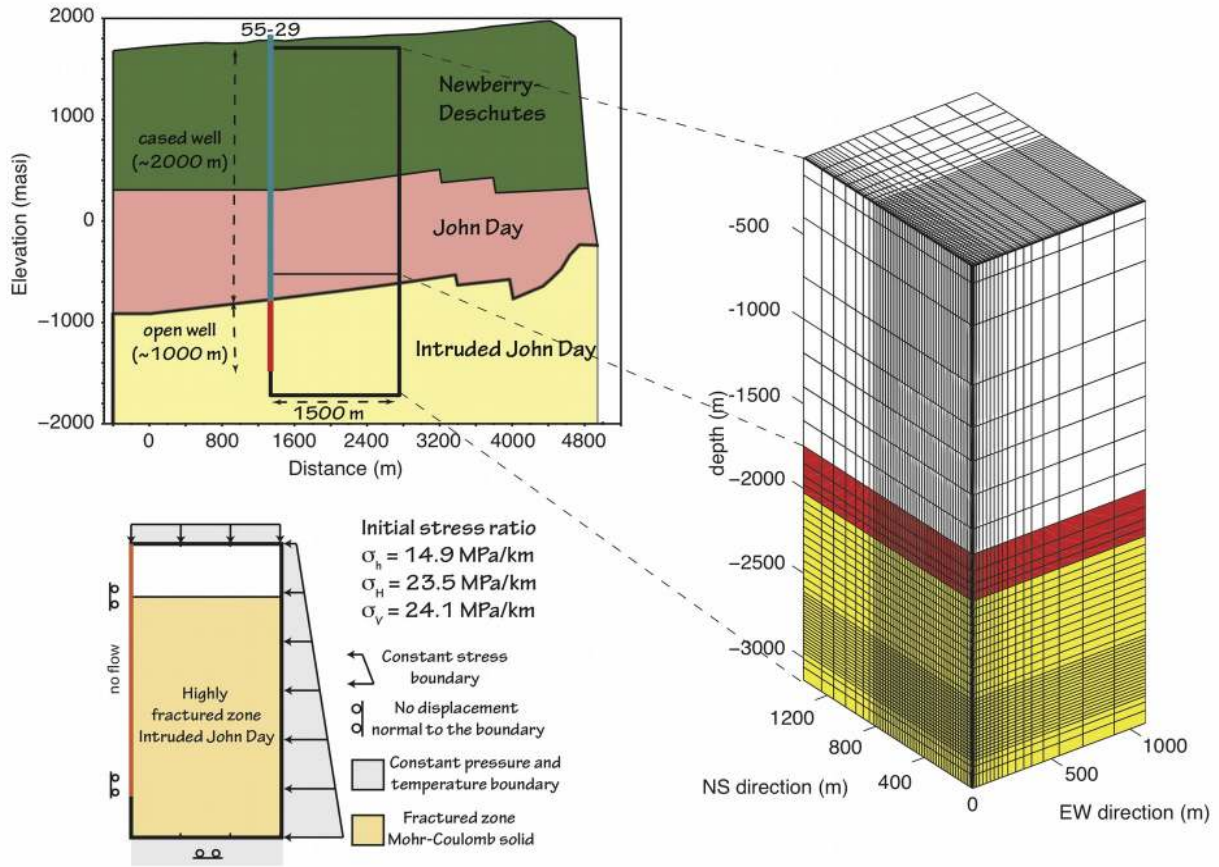
735

736*Figure 1*. Mesh and boundary conditions for modeling the stimulation of an EGS reservoir.

737Initial pressure, temperature and stress condition follows pre-stimulation analysis at the

738Newberry Volcano EGS Demonstration, as well as rock properties and distribution.

739
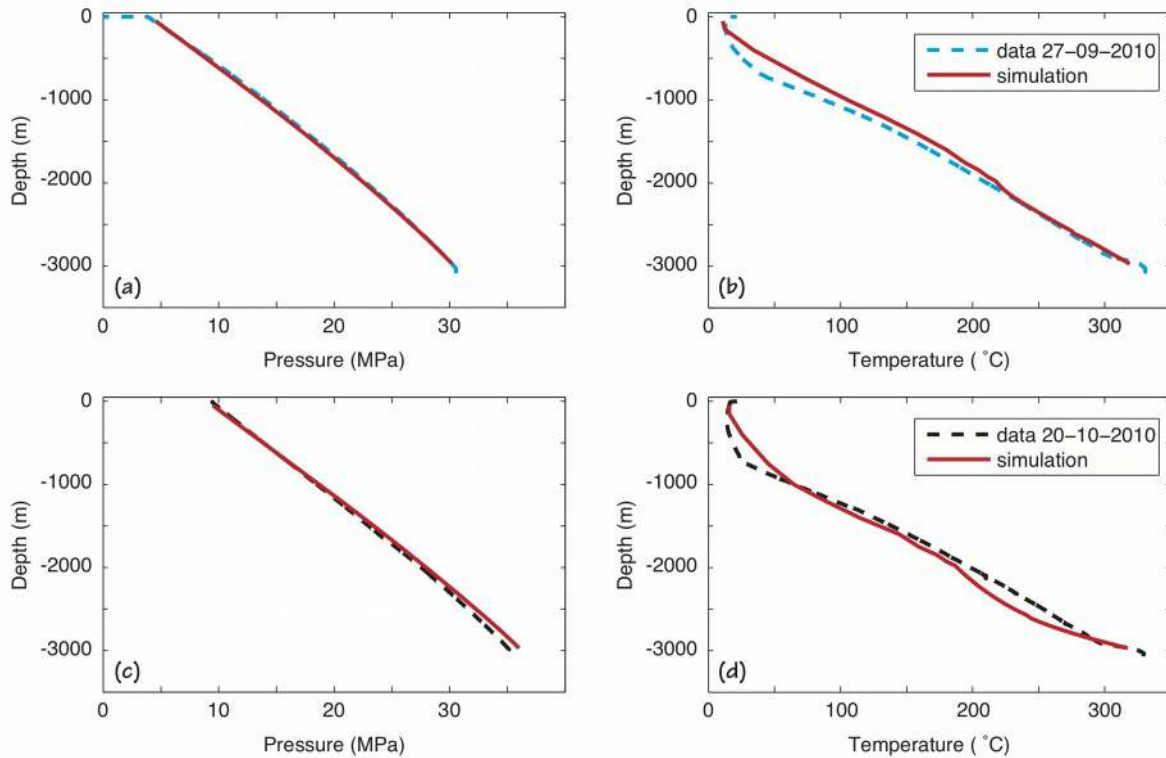
Figure 2. Model calibration. (a) Pressure well log (blue, dashed line) and simulated pressure (red 741line) after 3 days (09/27/2010) of 0.6 kg/s (10 gpm) injection rate. (b) Temperature well log 742(blue, dashed line) and simulated temperature (red line) after 3 days (09/27/2010) of 0.6 kg/s (10 743gpm) injection rate. (c) Pressure well log (black, dashed line) and simulated pressure (red line) 744after 9 days (10/20/2010) of 1.4 kg/s (22 gpm) injection rate. (d) Temperature well log (blue, 745dashed line) and simulated temperature (red line) after 9 days (10/22/2010) of 1.4 kg/s (22 gpm) 746injection rate.
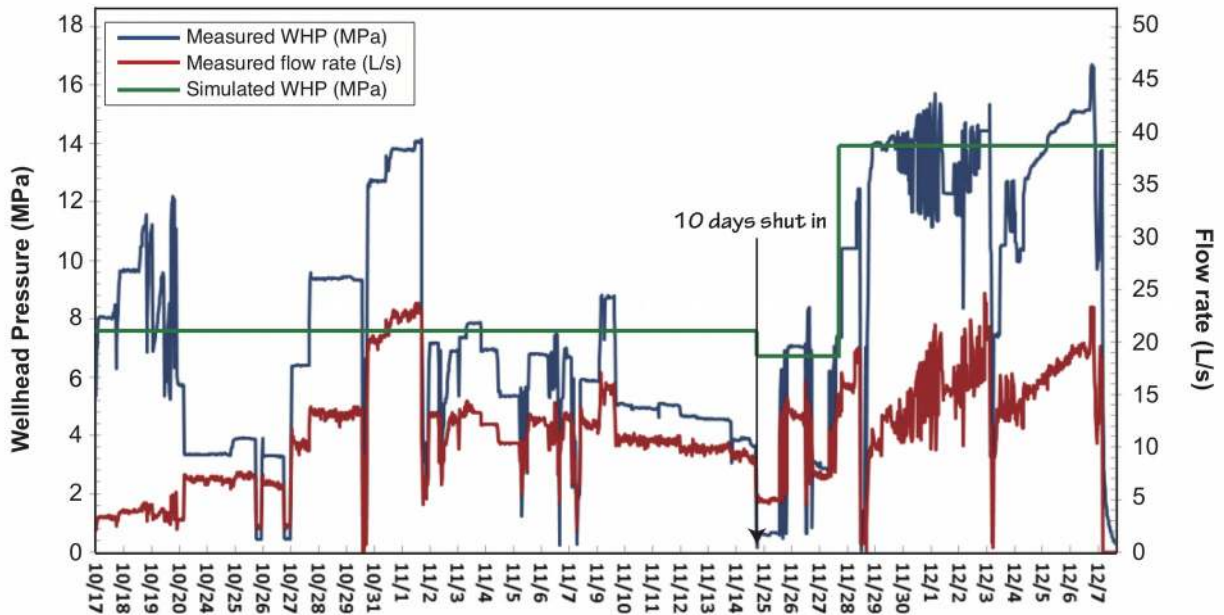
747

748*Figure 3*. Example of stimulation. Wellhead pressure (blue) and injection rate (red) observed at

749Newberry Volcano EGS Demonstration. Gap in timeline is when stimulation pumps were offline.

750The green line represents an average of the wellhead pressure, which is used as input for our

751modeling of an EGS system to study the hydroshearing. The shut in period between our first and

752second stage is indicated in figure. Note that at Newberry during that period the injection

753continued at a very low rate.
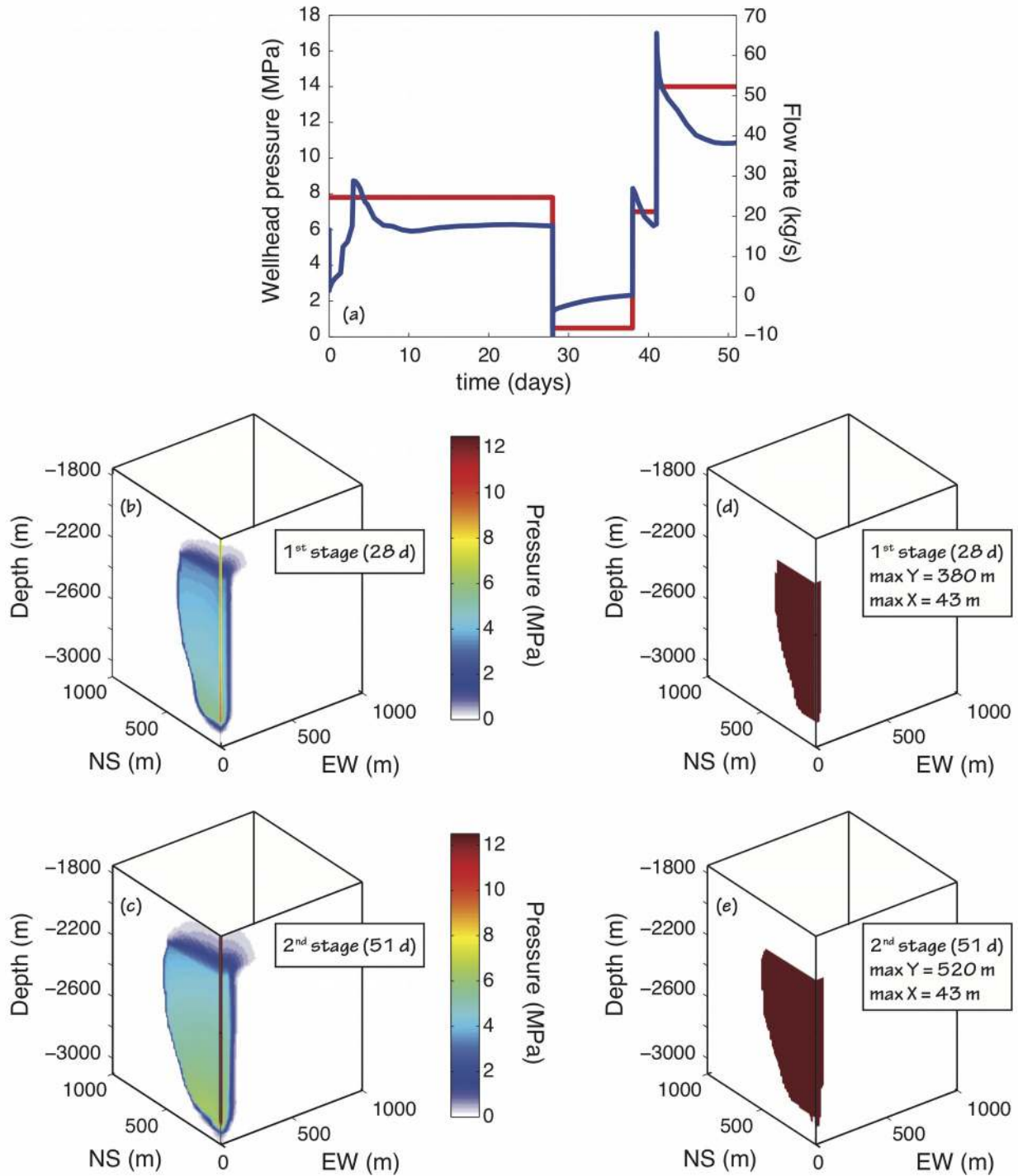
754

755 *Figure 4*. Simulation results for a system fully saturated with water. (a) Applied wellhead

756 pressure (red) and resulting flow rate (blue). (b, c) Resulting pressure and hydrosheared zone at

757 the end of the first stage (28 days). (d, e) Resulting pore pressure changes and hydrosheared zone

758 at the end of the second stage (51 days).

36   37
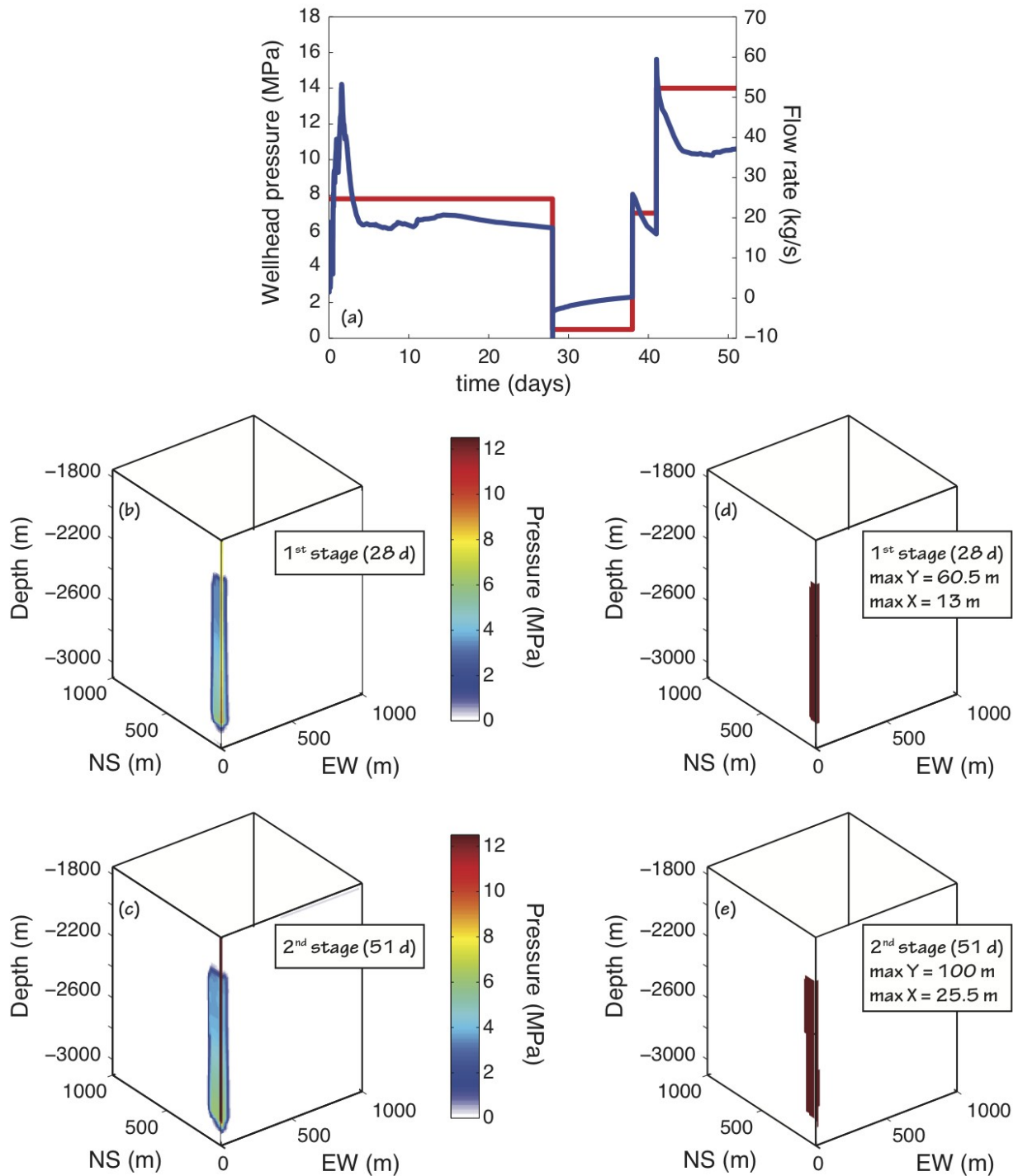
759

760Figure 5. Simulation results for a system initially saturated with carbon dioxide. (a) Applied

761wellhead pressure (red) and resulting flow rate (blue). (b, c) Resulting pressure and hydrosheared

762zone at the end of the first stage (28 days). (d, e) Resulting pore pressure changes and

763hydrosheared zone at the end of the second stage (51 days).

37   38
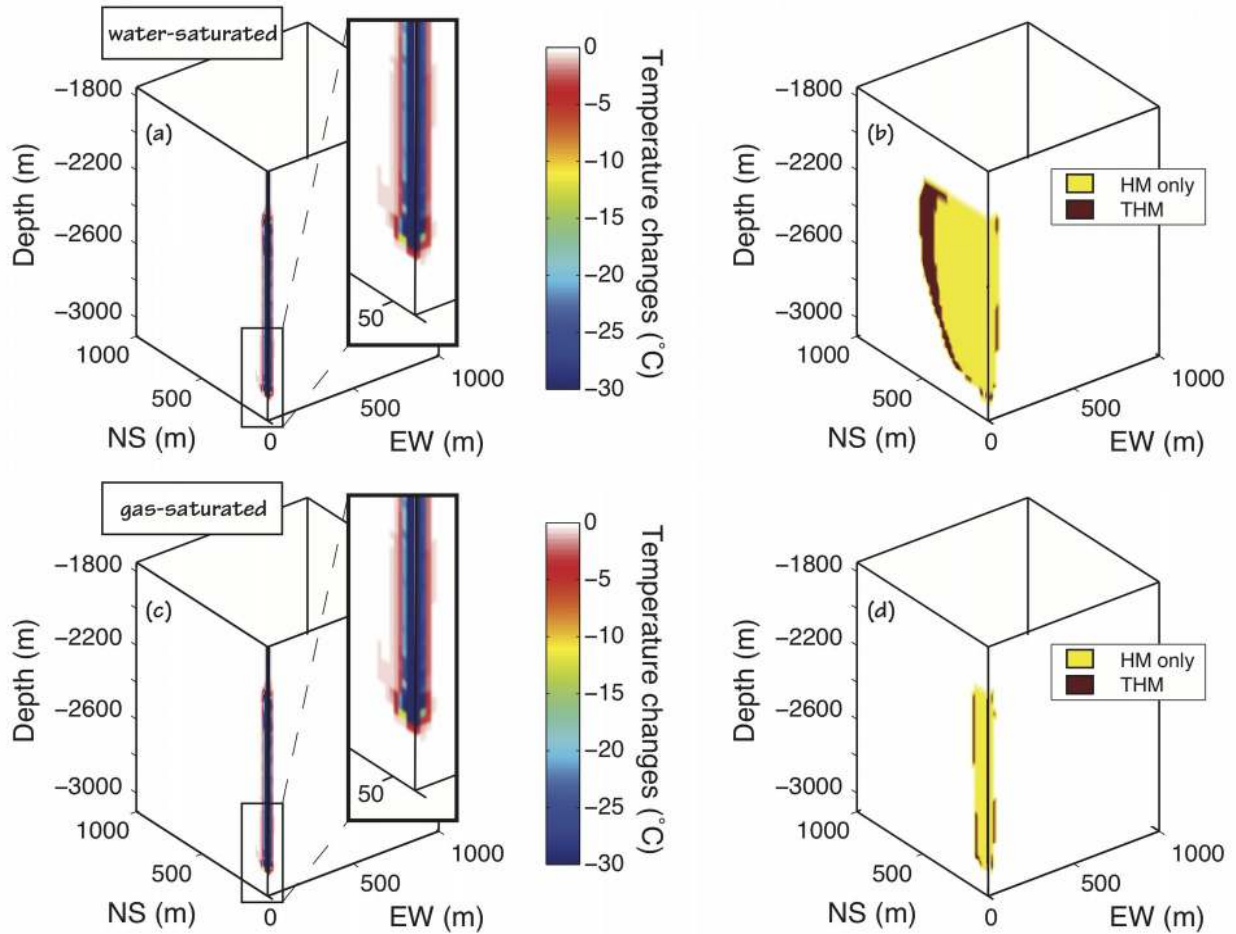
764

765*Figure 6*. (a) Temperature changes after the stimulation and (b) resulting hydrosheared zone for

766THM (brown) and HM (yellow) modeling for a water-saturated system. (c) Temperature changes

767after the stimulation and (d) resulting hydrosheared zone for THM (brown) and HM (yellow)

768modeling for a system initially fully saturated with gas.
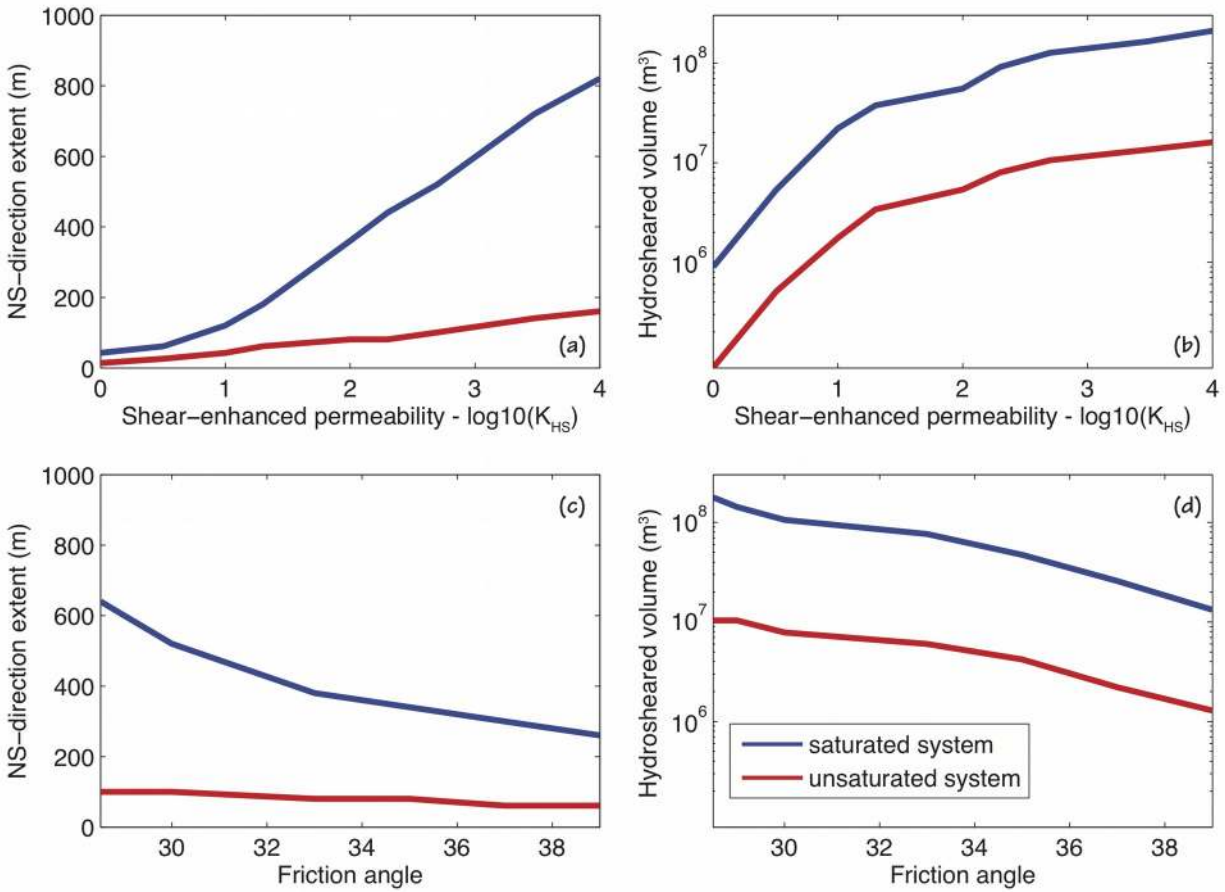
769

770*Figure 7*. Sensitivity analysis. Blue and red lines refer to saturated and unsaturated systems,

771respectively. EGS reservoir extent along NS-direction (a) and hydrosheared volume (b) as a

772function of the constant for shear-enhanced permeability (K_{HS}, Eq. 6). EGS reservoir extent along

773NS-direction (c) and hydrosheared volume (d) as a function of the friction angle for the Mohr

774Coulomb criterion (, Eq. 7).

775